

Information channels in protein interaction networks

Aleksandar Stojmirović and Yi-Kuo Yu*

National Center for Biotechnology Information
National Library of Medicine
National Institutes of Health
Bethesda, MD 20894
United States

Abstract

Motivation:

Recent advances in experimental techniques have generated large amounts of protein interaction data, producing networks containing large numbers of cellular proteins. Mathematically sound and robust foundations are needed for extensive, context-specific exploration of networks, integrating knowledge from different specializations and facilitating biological discovery.

Results:

Extending our earlier work, we present a theoretical construct, based on random walks, for modelling information channels between selected points in interaction networks. The software implementation, called *ITM Probe*, can be used as a network exploration and hypothesis forming tool. Through examples involving the yeast pheromone response pathway, we illustrate the versatility and stability of *ITM Probe*.

Availability:

www.ncbi.nlm.nih.gov/CBBresearch/qmbp/itm_probe

Contact:

yyu@ncbi.nlm.nih.gov

*to whom correspondence should be addressed

1 Introduction

Protein interaction networks are presently the subject of intensive and wide-ranging research (Bader *et al.*, 2008). Recently, a number of authors have applied the concepts of information flow and random walks to extract biologically relevant information from protein interaction networks (Nabieva *et al.*, 2005; Tu *et al.*, 2006; Suthram *et al.*, 2008). We have also developed a mathematical framework for information flow in interaction networks (Stojmirović and Yu, 2007). In this paper, we present a major extension of our previous framework, which permits natural modelling of channeled flow through networks.

Our framework models information flow in interaction networks through discrete random walks. Each random walk simulates a possible information path. A walker starts at a node in the network and at each discrete time step moves randomly to a neighboring node. The probability of moving to a particular neighboring node is proportional to the weight of the link from the present node to it. Unlike the classical random walks, our model allows the walker a certain probability to *dissipate*, that is, to leave the network at each step. Each walk terminates either by dissipation or by reaching a destination node.

The software implementation, founded upon our theoretical ideas, can in principle integrate existing partial knowledge to form a broad picture of possible communication paths in cellular processes. Hence, it can be used as a hypothesis forming tool and may help in delineating possible directions for future experiments. The salient feature of our method is its ability to provide context-specific analysis.

This paper is structured as follows. Section 2 presents an overview of our previous work and introduces the notion of a *channel tensor*. Section 3 describes the software implementation of the theory, called *ITM Probe*. Section 4 uses the yeast pheromone response pathway to exhibit several aspects of *ITM Probe* and is followed by discussion and future directions in Sections 5 and 6, with more technical details in the Appendix.

2 Theory

2.1 Preliminaries

We will closely follow the notation from our earlier paper (Stojmirović and Yu, 2007), expanding on it where necessary. We represent an interaction network as a weighted directed graph $\Gamma = (V, E, w)$ where V is a finite set of vertices of size n , $E \subseteq V \times V$ is a set of edges and w is a non-negative real-valued function on $V \times V$ that is positive on E , giving the weight of each edge (the weight of non-existing edge is defined to be 0). Assuming an ordering of vertices in V , we represent a real-valued function on V as a state (column) vector $\varphi \in \mathbb{R}^n$ and the connectivity of Γ by the *weight* matrix \mathbf{W} where $W_{ij} = w(i, j)$ (the weight of an edge from i to j). If Γ is an unweighted undirected graph, \mathbf{W} is the adjacency matrix of Γ where

$$W_{ij} = \begin{cases} 2 & \text{if } i = j \text{ and } (i, i) \in E, \\ 1 & \text{if } i \neq j \text{ and } (i, j) \in E, \\ 0 & \text{if } (i, j) \notin E. \end{cases} \quad (1)$$

We do not make distinction between a vertex $v \in V$ and its corresponding state given by a particular ordering of vertices. Denote by \mathbf{P} the $n \times n$ matrix such that

$$P_{ij} = \frac{\alpha_i W_{ij}}{\sum_k W_{ik}}, \quad (2)$$

where $\alpha_i \in (0, 1]$ for all i .

When $\alpha_i = 1$ for all i , the matrix \mathbf{P} is a transition matrix for a random walk or a Markov chain on Γ : for any pair of vertices i and j , P_{ij} gives the transition probability from vertex i to vertex j in one time step. In the general

case, the node-specific damping factors α_i model *dissipation* of information: at each step of the random walk there is a probability that the walk leaves the graph. The value α_i measures the likelihood for the random walk leaving the vertex i to remain in the graph.

2.2 Emitting and absorbing modes

We aim to discover the properties of information flow through a given network by examining the paths of discrete random walks. A random walker starts at an originating node, chosen according to the application domain, and traverses the network, visiting a node at each step. Each walk terminates at an explicit *boundary* vertex or due to dissipation, which is modelled as reaching an implicit (out-of-network) boundary node.

We distinguish two types of boundary nodes: *sources* and *sinks*. Sources emit information, that is, serve as the origins of random walks. All information entering a source from inside the network is dissipated, so a walker is not allowed to visit the source more than once. Sinks absorb information, serving as destinations of walks; information leaving each sink is dissipated. The network graph together with a set of boundary nodes and a vector of damping factors α provides the *context* for the information flow being investigated.

The main variable of interest is the (averaged) number of times a vertex is visited by a random walk given the context. Let D denote the set of selected boundary nodes, let $T = V \setminus D$ and let $m = |T|$. Assuming that the first $n - m$ states correspond to vertices in D , we write the matrix \mathbf{P} in the canonical block form:

$$\mathbf{P} = \begin{bmatrix} \mathbf{P}_{DD} & \mathbf{P}_{DT} \\ \mathbf{P}_{TD} & \mathbf{P}_{TT} \end{bmatrix}. \quad (3)$$

Here \mathbf{P}_{AB} denotes a matrix giving probabilities of moving from A to B where A, B stand for either D or T . The states (vertices) belonging to the set T are called *transient*.

2.2.1 Absorbing mode

Suppose that the boundary set D consists only of sinks. Let \mathbf{F} denote an $m \times (n - m)$ matrix such that F_{ij} is the total probability that the information originating at $i \in T$ is absorbed at $j \in D$. The matrix \mathbf{F} is found by solving the discrete Laplace equation

$$(\mathbb{I} - \mathbf{P}_{TT})\mathbf{F} = \mathbf{P}_{TD}, \quad (4)$$

where \mathbb{I} denotes the identity matrix. The matrix $\Delta = \mathbb{I} - \mathbf{P}_{TT}$ is known as the discrete Laplace operator of the matrix \mathbf{P}_{TT} . If $\mathbb{I} - \mathbf{P}_{TT}$ is invertible, Equation (4) has a unique solution

$$\mathbf{F} = \mathbf{G}\mathbf{P}_{TD}, \quad (5)$$

where $\mathbf{G} = (\mathbb{I} - \mathbf{P}_{TT})^{-1}$.

2.2.2 Emitting mode

Now consider the dual problem where D is a set of sources. Let \mathbf{H} denote an $(n - m) \times m$ matrix such that H_{ij} is the total expected number of times the transient vertex j is visited by a random walk emitted from source i (for all times). Again, \mathbf{H} is found by solving the discrete Laplace equation

$$\mathbf{H}(\mathbb{I} - \mathbf{P}_{TT}) = \mathbf{P}_{DT}. \quad (6)$$

which, if $\mathbb{I} - \mathbf{P}_{TT}$ is invertible, has a unique solution

$$\mathbf{H} = \mathbf{P}_{DT}\mathbf{G}. \quad (7)$$

It is easy to show (Stojmirović and Yu, 2007) that the matrix $\mathbf{G} = (\mathbb{I} - \mathbf{P}_{TT})^{-1}$ (also known as the Green's function) exists if $\alpha_i < 1$ for all i . This condition is not even necessary if the underlying graph Γ is connected. The entry G_{ij} represents the mean number of times the random walk reaches vertex $j \in T$ having started in state $i \in T$.

2.2.3 Interpretations

If we assume that a random walk deposits a fixed amount of information content each time it visits a node, we can interpret H_{ij} as the overall amount of information content originating from the source i deposited at the transient vertex j . Furthermore, we can interpret F_{ij} as the sum of probabilities (weights) of the paths originating at the vertex $i \in T$ and terminating at the vertex $j \in D$ that avoid all other nodes in the set D , and H_{ij} as the sum of probabilities (weights) of the paths originating at the vertex $i \in D$ and terminating at the vertex $j \in T$, also avoiding all other nodes in the set D . Each such path has a finite but unbounded length. However, unlike F_{ij} , H_{ij} does not represent a probability because the events of the information being located at j at the times t and t' are not mutually exclusive (a random walk can be at j at time t and revisit it at time t'). For F_{ij} , the absorbing events at different times are mutually exclusive.

2.3 Channel mode

In the absorbing and emitting modes as above, the sources and sinks are kept separate, that is, the absorbing mode only supports sinks while the emitting mode only supports sources. In (Stojmirović and Yu, 2007) we introduced *pseudosinks* to the emitting mode to overcome this problem. Pseudosinks are transient nodes that dissipate all (or most) walks leaving them. An additional practical difficulty in using the above modes is that very few walks reach the selected destinations (i.e. sinks or pseudosinks), most being dissipated. To direct the flow towards the destinations, we used the potential functions to redistribute the weights of edges of the original graph so that paths moving closer to the destinations are favored over those moving away from them. While our model provided very reasonable results on many examples from yeast protein-protein interaction networks, it also suffered from several problems. The choice of the potentials was purely empirical since there was no theoretical foundation for any particular form they should take. Furthermore, the underlying graph is slightly different for each choice of the boundary and destination sets, hindering rapid computation at large-scale.

A way to overcome the above problems is to combine the absorbing and the emitting modes in such a way that the absorbing probabilities are used to select the paths from sources to sinks.

From now, assume $V = S \sqcup T \sqcup K$, where the set S denotes the sources, K denotes the sinks and T the transient nodes and write the matrix \mathbf{P} in the block form as

$$\mathbf{P} = \begin{bmatrix} \mathbf{P}_{SS} & \mathbf{P}_{ST} & \mathbf{P}_{SK} \\ \mathbf{P}_{TS} & \mathbf{P}_{TT} & \mathbf{P}_{TK} \\ \mathbf{P}_{KS} & \mathbf{P}_{KT} & \mathbf{P}_{KK} \end{bmatrix}. \quad (8)$$

We will modify (add context to) the underlying graph Γ so that the random walk can only leave the sources and only enter the sinks (no communication is allowed between sources or between sinks). The modified transition matrix, denoted $\tilde{\mathbf{P}}$ has the form

$$\tilde{\mathbf{P}} = \begin{bmatrix} \mathbf{0} & \mathbf{P}_{ST} & \mathbf{P}_{SK} \\ \mathbf{0} & \mathbf{P}_{TT} & \mathbf{P}_{TK} \\ \mathbf{0} & \mathbf{0} & \mathbf{0} \end{bmatrix}. \quad (9)$$

Treating the vertices in S and T as transient for the absorbing mode in 2.2.1, we first derive the matrix \mathbf{F} (of size $|S \cup T| \times |K|$):

$$\begin{aligned} \mathbf{F} &= \left(\mathbb{I} - \begin{bmatrix} \mathbf{0} & \mathbf{P}_{ST} \\ \mathbf{0} & \mathbf{P}_{TT} \end{bmatrix} \right)^{-1} \begin{bmatrix} \mathbf{P}_{SK} \\ \mathbf{P}_{TK} \end{bmatrix} \\ &= \begin{bmatrix} \mathbb{I} & \mathbf{P}_{ST}\mathbf{G} \\ \mathbf{0} & \mathbf{G} \end{bmatrix} \begin{bmatrix} \mathbf{P}_{SK} \\ \mathbf{P}_{TK} \end{bmatrix} \\ &= \begin{bmatrix} \mathbf{P}_{SK} + \mathbf{P}_{ST}\mathbf{G}\mathbf{P}_{TK} \\ \mathbf{G}\mathbf{P}_{TK} \end{bmatrix}, \end{aligned}$$

where, as before, $\mathbf{G} = (\mathbb{I} - \mathbf{P}_{TT})^{-1}$.

Similarly, treating the vertices in T and K as transient for the emitting mode in 2.2.2, we derive the matrix \mathbf{H} (of size $|S| \times |T \cup K|$):

$$\begin{aligned} \mathbf{H} &= \begin{bmatrix} \mathbf{P}_{ST} & \mathbf{P}_{SK} \end{bmatrix} \left(\mathbb{I} - \begin{bmatrix} \mathbf{P}_{TT} & \mathbf{P}_{TK} \\ \mathbf{0} & \mathbf{0} \end{bmatrix} \right)^{-1} \\ &= \begin{bmatrix} \mathbf{P}_{ST} & \mathbf{P}_{SK} \end{bmatrix} \begin{bmatrix} \mathbf{G} & \mathbf{G}\mathbf{P}_{TK} \\ \mathbf{0} & \mathbb{I} \end{bmatrix} \\ &= \begin{bmatrix} \mathbf{P}_{ST}\mathbf{G} & \mathbf{P}_{ST}\mathbf{G}\mathbf{P}_{TK} + \mathbf{P}_{SK} \end{bmatrix}. \end{aligned}$$

The entries of \mathbf{F} and \mathbf{H} are, as before, interpreted as probabilities of absorption at sinks and average numbers of visits of walks emitted from sources, respectively. Note that the same Green's function, $\mathbf{G} = (\mathbb{I} - \mathbf{P}_{TT})^{-1}$, needs to be computed for both solutions. Also note that the ' S ' rows of \mathbf{F} form the transpose of the ' K ' columns of \mathbf{H} , that is, for all $s \in S$ and $k \in K$, $F_{sk} = H_{sk}$.

The matrices \mathbf{F} and \mathbf{H} can be extended into the matrices $\bar{\mathbf{F}}$ and $\bar{\mathbf{H}}$, of sizes $n \times |K|$ and $|S| \times n$, respectively (i.e. extended over the whole graph) by explicitly setting the S and K portions to the identity matrices:

$$\bar{\mathbf{F}} = \begin{bmatrix} \mathbf{P}_{SK} + \mathbf{P}_{ST}\mathbf{G}\mathbf{P}_{TK}, & \mathbf{G}\mathbf{P}_{TK}, & \mathbb{I} \end{bmatrix}^T \quad (10)$$

$$\bar{\mathbf{H}} = \begin{bmatrix} \mathbb{I}, & \mathbf{P}_{ST}\mathbf{G}, & \mathbf{P}_{ST}\mathbf{G}\mathbf{P}_{TK} + \mathbf{P}_{SK} \end{bmatrix} \quad (11)$$

In this way, we explicitly describe our assumptions that a random walk originating at each source can only leave it and not return to any source and that any random walk originating at a sink has probability 1 of staying there.

2.3.1 Channel tensor

Define the *channel tensor* $\Phi \in V \otimes K \otimes S^*$ by

$$\Phi_{i,k}^s = \bar{H}_{si} \bar{F}_{ik}. \quad (12)$$

It can be easily shown that the value of $\Phi_{i,k}^s$ gives the expected number of times a random walk emerging from the source s and terminating at the sink k visits the vertex i . Furthermore, from Equations (10–11), one can easily see that for all $s \in S$ and $k \in K$,

$$\Phi_{s,k}^s = \Phi_{k,k}^s, \quad (13)$$

which supports the above interpretation. The values of Φ depend on the values of the damping factors α_j for all $j \in V$.

Let $\Psi_s = \sum_{k' \in K} \Phi_{s,k'}^s$ denote the expected number of times a random walk emerging from the source s reaches any of the sinks. Define the *normalized channel tensor*, $\hat{\Phi} \in V \otimes K \otimes S^*$ by

$$\hat{\Phi}_{i,k}^s = \frac{\Phi_{i,k}^s}{\Psi_s}. \quad (14)$$

The normalized channel tensor $\hat{\Phi}_{i,k}^s$ gives the expectation of the number of visits of i by a random walk from s to k , conditional on the random walk being terminated at sinks only. Equations (13-14) imply that for all $s \in S$,

$$\sum_{k \in K} \hat{\Phi}_{k,k}^s = \sum_{k \in K} \hat{\Phi}_{s,k}^s = 1. \quad (15)$$

It can be shown that for undirected graphs, with a context consisting of a single source and a single sink, the values of $\hat{\Phi}$ are invariant under interchange of sources and sinks. In general, however, reversing sources and sinks

gives a different result, both due to asymmetry of the weight matrix in directed graphs and because sources and sinks have different roles if more than one of each are present. Random walkers originating from different sources can simultaneously visit a transient node while a walk can terminate only at a single sink. Thus, the sinks split the total information flow, that is, compete for it, while sources interfere, either constructively or destructively (see 2.3.2 below).

The damping coefficients influence the normalized channel tensor differently from the non-normalized one or the absorbing and emitting solutions. For the non-normalized versions, damping factors control the amount of information reaching the boundary and any intermediate points. In the normalized case, we consider only the information having reached the sinks. The damping factors determine the paths taken by random walks as they move from sources to sinks. Small values strongly favor the nodes on the shortest paths, while large values allow random walks to take longer paths and hence favor the vertices with many connections. Appendix A contains a more detailed analysis of the role of damping factors in the channel mode.

2.3.2 Summary functions

The (normalized) channel tensor provides a detailed view of information flow between sources and sinks within a context. However, for practical applications, it is sometimes desirable to reduce the amount of available information to a single vector over V , which can be tabulated and graphically visualized using color maps. The summary quantities that we present below are based on those developed for the emitting model in (Stojmirović and Yu, 2007) with some modifications.

The *source specific content* of a normalized channel tensor $\hat{\Phi}$, denoted $\hat{\phi}^s$ is a quantity that for each node $i \in V$ assigns the total number of visits of a random walk originating from a source $s \in S$, that is,

$$\hat{\phi}_i^s = \sum_{k \in K} \hat{\Phi}_{i,k}^s. \quad (16)$$

The *total content* of $\hat{\Phi}$, denoted by $\hat{\tau}$, sums all visits for each node: $\hat{\tau}_i = \sum_{s \in S} \hat{\phi}_i^s$. The concept of *destructive interference* measures at each node the overlap between visits from different sources. We define the interference vector $\hat{\sigma}$ over V by

$$\hat{\sigma}_i = |S| \min_{s \in S} \hat{\phi}_i^s. \quad (17)$$

Hence, $\hat{\sigma}_i$ gives the total number of times the random walks from all sources co-occur at each node (scaled by the number of sources).

With damping factors less than unity, the random walks from sources to sinks effectively visit a small portion of the entire underlying network. Information Transduction Module or ITM is a notion that we use to describe the set of nodes most influenced by the flow. The nodes are ranked using their values for the total content or interference and the most significant nodes are selected. The number of selected nodes depends on the application-specific considerations but we found that the *participation ratio* π (Stojmirović and Yu, 2007) of the total content vector $\hat{\tau}$ gives a good estimate of the number of nodes whose relative amount of content is significant. It is given by the formula

$$\pi(\hat{\tau}) = \frac{(\sum_{i \in V} \hat{\tau}_i)^2}{\sum_{j \in V} \hat{\tau}_j^2}. \quad (18)$$

3 ITM Probe

ITM Probe is a software implementation of our theoretical framework, written in the Python programming language and available as a standalone library and as a web service. Its main utility is to extract information from protein interaction networks by using partial and local information (pairwise interactions), possibly coming from a variety of sources, to obtain a context-specific overview of possible information flow patterns.

At present, *ITM Probe* provides three models, channel, absorbing and emitting, corresponding to the modes from the previous section. The results are based on the source specific content for the channel and emitting model and on absorbing probabilities for the absorbing models. The web service has, due to interface considerations, more limited parameter sets: the damping factor is assumed constant for all nodes (henceforth denoted α) and the numbers of sources and sinks are limited.

3.1 Input parameters

ITM Probe requires as input the model, an interaction graph and the context parameters (sources, sinks and damping factors). The web service channel model allows up to three independent contexts to be specified, allowing investigation of the overlap of independent channels through interference.

At present, the web service supports only the yeast physical interaction networks derived from the BIOGRID (Stark *et al.*, 2006) database – we intend to eventually make available the networks from other model organisms. Our network graphs consist only of those interactions that are from low-throughput experiments (that is, from publications reporting less than 300 interactions) or are reported by at least two independent publications. We provide a version of the yeast network where the interactions labelled with ‘Biochemical activity’ are considered as directed links (bait \rightarrow prey) as well as a graph where all edges are undirected.

It is well known (Steffen *et al.*, 2002) that proteins with a large number of non-specific interaction partners might overtake the true signaling proteins in the information flow modeling. Therefore, *ITM Probe* allows users to specify nodes to exclude from the network. For the yeast network the nodes excluded by default include cytoskeleton proteins, histones and chaperones, since they may provide undesirable shortcuts.

The emitting model also allows setting the destinations of information and the potentials that modify the network to attract the flow from sources to them. These options are now rendered obsolete by the channel model and serve only to illustrate the concepts from our earlier paper. The potentials directing the flow towards sinks can also be set for the absorbing model.

3.2 Output

The output of the web version of *ITM Probe* consists of the graphical representation of the resulting ITM, query-related summary statistics and a table listing the top ranking members of the ITM (Fig. 1). Each row of the table contains the protein name, the associated model values and the links to selected databases containing the descriptions of the protein.

The graphical representation shows the sub-network of most significant nodes from the resulting ITM, laid out according to a layout seed (every seed produces a different drawing of the same sub-network). The table shows only the nodes shown in the graphical display but the full model solution can be downloaded in the CSV format for further analysis.

The nodes comprising an ITM are selected according to the total content (emitting and channel models) or the total likelihood of reaching a sink (absorbing model). The number of nodes to be shown is either specified directly or determined through a criterion such as participation ratio or the cutoff value.

Each graphical layout can be rendered and saved in multiple formats (SVG, PNG, JPEG, EPS and PDF). Images of large sub-networks in SVG format can be navigated online using the ‘Network Navigator’ applet. For each rendering, the users can choose which aspects of results to display, the color map and the scale for presentation (linear or logarithmic). When multiple boundary points are specified, it is possible to obtain an overview of all flows simultaneously by selecting the color mixture scheme (Fig. 1). In this case, each source (in the channel or emitting model) or sink (in the absorbing model) is assigned a basic CMY (cyan, magenta or yellow) color and the coloring of each displayed node is a result of mixing the colors corresponding to its source- or sink- specific values for each of the boundary points.

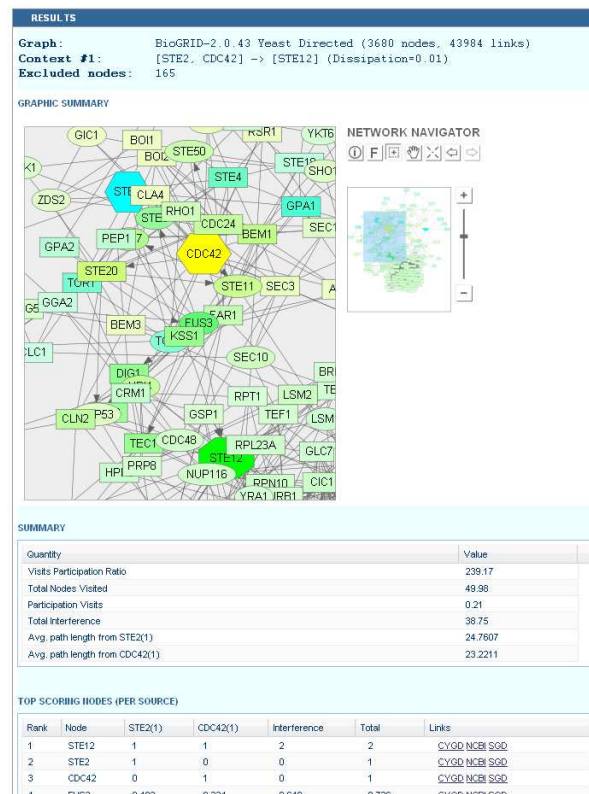


Figure 1: A partial screenshot of the results of the *ITM Probe* web service.

4 Examples: Yeast Pheromone Pathway

For our examples, we use the mating pheromone response pathway in *Saccharomyces cerevisiae*, the one of the best understood signalling pathways in eukaryotes (Bardwell, 2005). The mating signal is transferred from a membrane receptor to a transcription factor in nucleus, leading to transcription of mating genes. We will only provide a very brief overview of the pathway necessary for discussing our examples; more details are available in the review by Bardwell (2005).

A mating pheromone binds the transmembrane G-protein coupled pheromone receptors Ste2p/Ste3p. This leads to dissociation of Ste4p and Ste18p, the membrane bound subunits of the G-protein complex, which also contains the subunit Gpa1p. Ste4p then binds to the protein kinase Ste20p, which is recruited to the membrane through Cdc42p, and the scaffold protein Ste5p. On the scaffold, a MAPK (mitogen activated protein kinase) cascade occurs, where each protein kinase in a cascade is activated by being phosphorylated by the previous kinase and in turn activates the next protein. In this case, the cascade goes Ste20p → Ste11p → Ste7p → Fus3p or Kss1p. The final activated kinase Fus3p or Kss1p then migrates to the nucleus where it phosphorylates the proteins Dig1p and Dig2p, the repressors of the Ste12p transcription factor activity. The Ste12p transcription factor can then, in coordination with other transcription factors such as Tec1p, promote the transcription of the mating genes.

As the underlying network, we use the BIOGRID-2.0.43 interactions, filtered in favor of low-throughput interactions as described in 3.1. The physical binding interactions are given a weight 1.0 in both directions while the biochemical activity interactions are interpreted as directional and given a weight of 2.0 (where both physical and bio-

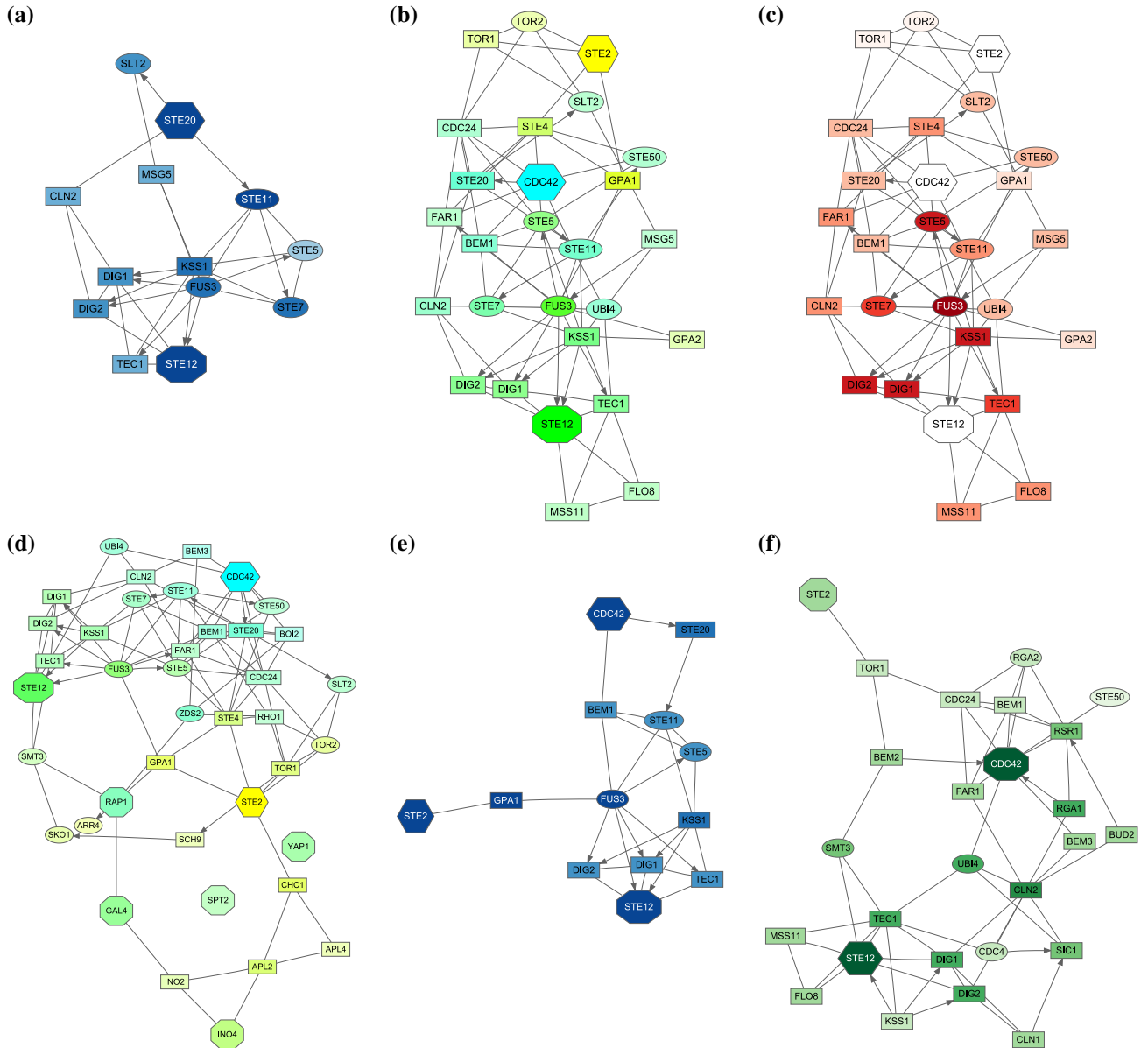


Figure 2: Yeast pheromone response ITMs: in each case we report the context described as $\{\text{sources}\} \rightarrow \{\text{sinks}\} (\alpha)$. The number of nodes shown is determined by the participation ratio in all cases except **(d)**, where only 40 top ranking nodes are shown due to space constraints. The parts **(a)**, **(e)** and **(f)** are colored by the total content, **(b)** and **(d)** by source specific content (color mixture) and **(c)** by interference. Contexts: **(a)** $\{\text{Ste20p}\} \rightarrow \{\text{Ste12p}\} (0.85)$; **(b)** $\{\text{Ste2p, Cdc42p}\} \rightarrow \{\text{Ste12p}\} (0.85)$; **(c)** $\{\text{Ste2p, Cdc42p}\} \rightarrow \{\text{Ste12p}\} (0.85)$; **(d)** $\{\text{Ste2p, Cdc42p}\} \rightarrow \{\text{Ste12p, Gal4p, Ino4p, Ume6p, Yap1p, Rap1p}\} (0.85)$; **(e)** $\{\text{Ste2p, Cdc42p}\} \rightarrow \{\text{Ste12p}\} (0.55)$; **(f)** $\{\text{Ste12p}\} \rightarrow \{\text{Ste2p, Cdc42p}\} (0.85)$.

chemical interactions are reported, only biochemical are considered). We used a set of 165 excluded nodes, consisting of histones, chaperones and cytoskeletal proteins. We found that the excluded nodes do not strongly affect the results of the particular examples presented here.

Fig. 2(a) focuses solely on the MAPK cascade portion of the pheromone pathway, with Ste20p as a single source and Ste12p as a single sink. Selection of top proteins by participation ratio captures all important participants of the cascade plus the proteins that do not play a direct role but interact with the most relevant ones (Slt2p, Cln2p). To obtain an ITM best describing the entire pheromone response pathway, it is necessary to include two sources, the receptor Ste2p and the membrane-bound protein Cdc42p (Fig. 2(b,c)). Including only Ste2p is not sufficient because of the shortcut through the link Gpa1p \rightarrow Fus3p, which avoids the MAPK cascade. Furthermore, inclusion of Cdc42p is biologically sensible because Cdc42p activates Ste20p and is hence necessary for the MAPK cascade. Interference between the information flows from Ste2p and Cdc42p (Fig. 2(c)), rather than total visits, highlights the most important proteins in the pathway.

The channel model is relatively robust to addition of non-relevant sinks to its contexts. In Fig. 2(d), we added five more transcription factor proteins as sinks, in addition to Ste12p. As can be seen, the most visited nodes mostly belong to the channel to Ste12p while the remaining sinks are linked to sources by weaker channels (mostly not shown because the figure shows only the top 40 nodes). In this case, Ste12p has 0.77 total visits (out of 2) with interference of 0.74. The remaining 1.23 visits are distributed among the other five sinks.

The importance of the choice of damping factors has been emphasised in the theoretical sections and in Appendix A. For example, setting $\alpha = 0.99$ with Cdc42p and Ste2p as sources and Ste12p as a sink, as shown in the screenshot from Fig. 1, leads to participation ratio of 239 and average path lengths of about 24 (the values are similar for both sources), that is, a random walk emanating from one of the sources visits on average 23 proteins before reaching Ste12p (the values for $\alpha = 0.85$ are 27 for the participation ratio and about 7 for both average path lengths). On the other hand, small values of α (Fig. 2(e)) lead to only the shortest paths being significant. The *ITM Probe* default value of $\alpha = 0.85$ gives, in our experience, the best results in emphasising biologically relevant channels.

Fig. 2(f) shows the effects of reversing sources and sinks. The resulting ITM performs much worse in describing the pheromone pathway for both reasons mentioned in 2.3.1. Firstly, the pheromone response pathway is dominated by the MAPK phosphorylation cascade, which is in our case modelled by directed links. Secondly, since the sinks are competing, most of the information emitted from Ste12p is captured by Cdc42p, leaving little for Ste2p. This illustrates different semantic roles for sources and sinks in the channel mode that need to be taken into account when using *ITM Probe*.

5 Discussion

Applied to protein interaction networks, *ITM Probe* can be used for exploration of network graphs and as a hypothesis forming tool. The absorbing and emitting models can be used to glimpse the network neighbourhoods of selected nodes and hence provide a good view of protein complexes. The ITMs obtained by absorbing and emitting models centered at the same nodes are slightly different: the absorbing model can reveal relatively distant ‘leaf’ nodes linked to a sink by a nearly unique path while the emitting model favors highly connected clusters due to the ‘resonance’ effect they induce: a random walk enters a cluster and visits many of its nodes several times before leaving it.

The channel model can be employed for discovery of potential pathways linking certain proteins or biological functions associated with them. Multiple sources (perhaps in multiple contexts) together with interference can be used to investigate potential points of crosstalk between information channels, while a solution based on a carefully chosen set of competing sinks can propose a plausible biological explanation among several possible ones.

We emphasize that when using *ITM Probe* as a discovery tool, it is up to the user to select the model context according to the biological context investigated and to verify the results afterwards. The choice of interaction graphs and excluded nodes is critical because of sensitivity of random walk frameworks to shortcuts and because interaction graphs by necessity do not capture the entire biochemical environment within the cell. Therefore, it is desirable to

select high-quality data relevant to the biological process under investigation. For example, a particular link, even if thoroughly experimentally verified, may have to be removed from the network if it corresponds to an interaction that does not occur in conjunction with other interactions relevant for the selected biological process.

Use of damping factors gives an advantage to our framework over similar models proposed based on random walks (Tu *et al.*, 2006), or equivalently, electrical networks (Suthram *et al.*, 2008). Dissipation, controlled by the user, focuses random walks to the portion of the network relevant to the context, preventing visits to distant nodes. Computationally, obtaining a solution involves simply a solution to a (sparse) system of linear equations, without necessity for any simulations of random walks as by Tu *et al.* (2006). For large scale computations using the same graph and damping factors but different boundaries, it is possible to reuse a previously computed solution (Appendix B) for computation of a new solution. This technique can lead to a significant speed-up for large networks.

6 Future directions

The mathematical framework presented here is flexible and can be applied and extended in a number of ways. We intend to apply it to physical interaction networks from more species, such as *Homo sapiens* and, beyond that, to metabolic or genetic networks, or a combination of networks of different types.

In another direction, we plan to extend the framework so that it is able to take into account additional biological information, if available. Such data includes protein complex memberships, activation states and their triggers as well as protein abundances. While these extensions may lead to nonlinear models, our aim is to preserve the simplicity of the present framework while improving accuracy. We see *ITM Probe* primarily as a discovery and hypothesis forming tool, rather than a detailed model of the cell.

Acknowledgments

This work was supported by the Intramural Research Program of the National Library of Medicine at National Institutes of Health.

ITM Probe implementation relies on a variety of open source components, which we acknowledge on our website. The color maps for network images were obtained from www.ColorBrewer.org. Graphic design of the website was done in collaboration with Zvezdana Stojmirović.

References

- Bader, S. *et al.* (2008). Interaction networks for systems biology. *FEBS Lett*, **582**(8), 1220–4.
- Bardwell, L. (2005). A walk-through of the yeast mating pheromone response pathway. *Peptides*, **26**(2), 339–50.
- Nabieva, E. *et al.* (2005). Whole-proteome prediction of protein function via graph-theoretic analysis of interaction maps. *Bioinformatics*, **21 Suppl 1**, 302–310.
- Poole, D. (2005). *Linear Algebra: A Modern Introduction*. Brooks Cole.
- Stark, C. *et al.* (2006). BioGRID: a general repository for interaction datasets. *Nucleic Acids Res*, **34**(Database issue), D535–9.
- Steffen, M. *et al.* (2002). Automated modelling of signal transduction networks. *BMC Bioinformatics*, **3**, 34.
- Stojmirović, A. and Yu, Y.-K. (2007). Information flow in interaction networks. *J Comput Biol*, **14**(8), 1115–43.
- Suthram, S. *et al.* (2008). eQED: an efficient method for interpreting eQTL associations using protein networks. *Mol. Syst. Biol.*, **4**, 162.

Tu, Z. *et al.* (2006). An integrative approach for causal gene identification and gene regulatory pathway inference. *Bioinformatics*, **22**, e489–496.

Appendix

A The role of the damping factor in the channel mode

Let \mathbf{W} be a weight matrix for a weighted connected graph $\Gamma = (V, E, w)$ and let α be a vector of positive coefficients over V such that $\alpha_i \leq 1$ for all $i \in V$. Let $\mu = \max_i \alpha_i$ and let $a_i = \alpha_i / \mu$. Then any transition matrix \mathbf{P} for Γ with dissipation given by α is given by $\mathbf{P} = \mu \mathbf{Q}$, where

$$Q_{ij} = \frac{a_i W_{ij}}{\sum_k W_{ik}}, \quad (19)$$

for all $i, j \in V$ by and $0 < a_i \leq 1$. As in the main text, let S, K and T be sets of sources, sinks and transient nodes, respectively, such that $V = S \sqcup K \sqcup T$.

From here onwards, we will consider μ as a free parameter in $(0, 1)$ and the transition matrix \mathbf{P} as dependent on μ . For this range of μ , the solution matrices $\bar{\mathbf{F}}$ and $\bar{\mathbf{H}}$ from Equations (10–11) are well defined, that is, the Green's function $\mathbf{G} = (\mathbb{I} - \mathbf{P}_{TT})^{-1} = \sum_{n=0}^{\infty} \mathbf{P}_{TT}^n$ is well-defined. As $\mu \downarrow 0$, all the damping factors in α uniformly tend to 0 and $\mathbf{P} \rightarrow \mathbf{0}$; however, as we will show, the normalized channel tensor is well-defined in the limit as $\mu \rightarrow 0$ (provided, of course, it is well defined for other values of μ). Note that, by construction, $\|\mathbf{Q}\|_{\infty} = 1$ and hence the solutions may not exist as $\mu \uparrow 1$ and $\mathbf{P} \rightarrow \mathbf{Q}$.

A.1 Path lengths

The damping parameter μ controls the distribution of lengths of the paths (or the times) a random walk emitted from a source takes before being absorbed at a sink.

For any $s \in S$, let L_s denote the random variable giving the length of the path (or a number of steps) taken by a random walk originating at s and terminating at any sink. The underlying probability density $\mathbb{P}(L_s = n)$ is given by

$$\mathbb{P}(n) = \frac{1}{\Psi_s} \begin{cases} \sum_{k' \in K} P_{sk'} & \text{for } n = 1; \\ \sum_{k' \in K} [\mathbf{P}_{ST} \mathbf{P}_{TT}^{n-2} \mathbf{P}_{TK}]_{sk'} & \text{for } n \geq 2. \end{cases} \quad (20)$$

We now compute closed forms for the mean and variance of L_s and discuss their dependence on μ . We require the following identities stated without proof:

$$\sum_{n=0}^{\infty} (n+2) \mathbf{P}_{TT}^n = \mathbf{G}^2 + \mathbf{G}, \quad (21)$$

$$\sum_{n=0}^{\infty} (n+2)^2 \mathbf{P}_{TT}^n = 2\mathbf{G}^3 + \mathbf{G}^2 + \mathbf{G}, \quad (22)$$

$$\frac{\partial}{\partial \mu} \mu^2 G_{ij} = \mu [\mathbf{G}^2 + \mathbf{G}]_{ij} \quad (23)$$

$$\frac{\partial}{\partial \mu} \mu^2 [\mathbf{G}^2]_{ij} = 2\mu [\mathbf{G}^3]_{ij}. \quad (24)$$

The first moment (the mean) of the distribution of L_s , $\mathbb{E}(L_s)$, is given by

$$\begin{aligned}\mathbb{E}(L_s) &= \frac{1}{\Psi_s} \sum_{k' \in K} \left(P_{sk'} + \sum_{n=0}^{\infty} (n+2) [\mathbf{P}_{ST} \mathbf{P}_{TT}^n \mathbf{P}_{TK}]_{sk'} \right) \\ &= \frac{1}{\Psi_s} \sum_{k' \in K} (P_{sk'} + [\mathbf{P}_{ST}(\mathbf{G} + \mathbf{G}^2) \mathbf{P}_{TK}]_{sk'})\end{aligned}\quad (25)$$

$$\begin{aligned}&= \frac{1}{\Psi_s} \sum_{k' \in K} (\hat{\Phi}_{s,k'}^s + [\mathbf{P}_{ST} \mathbf{G}^2 \mathbf{P}_{TK}]_{sk'}) \\ &= 1 + \sum_{k' \in K} \frac{[\mathbf{P}_{ST} \mathbf{G}^2 \mathbf{P}_{TK}]_{sk'}}{\Psi_s}\end{aligned}\quad (26)$$

$$\begin{aligned}&= 1 + \sum_{k \in K} \sum_{i \in T} \frac{H_{si} F_{ik}}{\Psi_s} \\ &= 1 + \sum_{k \in K} \sum_{i \in T} \hat{\Phi}_{i,k}^s,\end{aligned}\quad (27)$$

while the second moment $\mathbb{E}(L_s^2)$ is

$$\begin{aligned}\mathbb{E}(L_s^2) &= \frac{1}{\Psi_s} \sum_{k' \in K} \left(P_{sk'} + \sum_{n=0}^{\infty} (n+2)^2 [\mathbf{P}_{ST} \mathbf{P}_{TT}^n \mathbf{P}_{TK}]_{sk'} \right) \\ &= \frac{1}{\Psi_s} \sum_{k' \in K} (P_{sk'} + [\mathbf{P}_{ST}(\mathbf{G} + \mathbf{G}^2 + 2\mathbf{G}^3) \mathbf{P}_{TK}]_{sk'}) \\ &= \frac{2}{\Psi_s} \sum_{k' \in K} [\mathbf{P}_{ST} \mathbf{G}^3 \mathbf{P}_{TK}]_{sk'} + \mathbb{E}(L_s).\end{aligned}\quad (28)$$

The variance of L_s can therefore be computed using the standard formula $\text{Var}(L_s) = \mathbb{E}(L_s^2) - \mathbb{E}^2(L_s)$. The mean and the variance are related through μ :

Lemma 1. *Let $s \in S$. Then, for all $\mu \in (0, 1)$,*

$$\text{Var}(L_s) = \mu \frac{\partial}{\partial \mu} \mathbb{E}(L_s).\quad (29)$$

Proof. Let $X_{sk} = [\mathbf{P}_{ST} \mathbf{G}^2 \mathbf{P}_{TK}]_{sk}$. Then,

$$\frac{\partial}{\partial \mu} \mathbb{E}(L_s) = \sum_{k' \in K} \frac{\Psi_s \frac{\partial}{\partial \mu} X_{sk'} - X_{sk'} \frac{\partial}{\partial \mu} \Psi_s}{\Psi_s^2}.\quad (30)$$

Using Equation (24) we obtain

$$\begin{aligned}\frac{\partial}{\partial \mu} X_{sk} &= \sum_{i,j \in T} Q_{si} \frac{\partial}{\partial \mu} \mu^2 [\mathbf{G}^2]_{ij} Q_{jk} \\ &= \frac{2}{\mu} [\mathbf{P}_{ST} \mathbf{G}^3 \mathbf{P}_{TK}]_{sk},\end{aligned}\quad (31)$$

and, by Equations (23) and (25),

$$\begin{aligned}
\frac{\partial}{\partial \mu} \Psi_s &= \sum_{k' \in K} \left(Q_{sk'} + \sum_{i, j \in T} Q_{si} \frac{\partial}{\partial \mu} \mu^2 G_{ij} Q_{jk'} \right) \\
&= \frac{1}{\mu} \sum_{k' \in K} (P_{sk'} + [\mathbf{P}_{ST}(\mathbf{G} + \mathbf{G}^2)\mathbf{P}_{TK}]_{sk'}) \\
&= \frac{\Psi_s}{\mu} \mathbb{E}(L_s).
\end{aligned} \tag{32}$$

Therefore, by Equations (30) and (28),

$$\begin{aligned}
\mu \frac{\partial}{\partial \mu} \mathbb{E}(L_s) &= \frac{2}{\Psi_s} \sum_{k' \in K} [\mathbf{P}_{ST} \mathbf{G}^3 \mathbf{P}_{TK}]_{sk'} - \mathbb{E}(L_s) \sum_{k' \in K} \frac{X_{sk'}}{\Psi_s} \\
&= \mathbb{E}(L_s^2) - \mathbb{E}(L_s) - \mathbb{E}(L_s)(\mathbb{E}(L_s) - 1) \\
&= \text{Var}(L_s). \quad \square \qquad \square
\end{aligned}$$

A direct consequence of Lemma 1 is that $\mathbb{E}(L_s)$ is a continuous, increasing function of $\mu \in (0, 1)$. It is bounded from below: as $\mu \downarrow 0$, the variance of L_s vanishes, and, as will be shown in the remainder of this section, the average path-length converges to the length of the shortest path from the source to any of the sinks. The normalized channel tensor may be undefined for $\mu = 1$ (the Green's function \mathbf{G} need not exist) and in this case $\mathbb{E}(L_s)$ is unbounded as $\mu \uparrow 1$. If \mathbf{G} is well-defined for $\mu = 1$, then $\mathbb{E}(L_s)$ is bounded and attains its maximum at $\mu = 1$. The value of the maximum depends on the underlying network graph and the particular context.

A.2 Large dissipation asymptotics

For all $i, j \in V$, let $\rho(i, j)$ denote the (unweighted) length of the shortest directed path between i and j . We allow $\rho(i, j) = \infty$ if there exists no directed path between i and j . It is well-known that ρ is a (not necessarily symmetric) distance that satisfies the triangle inequality, that is, for all $i, j, k \in V$,

$$\rho(i, j) + \rho(j, k) \geq \rho(i, k). \tag{33}$$

For any source $s \in S$, let K_s denote the set of all points $k'' \in K$ such that for all $j \in K_s$ and every $k \in K \setminus K_s$, $\rho(s, j) < \rho(s, k)$. The set K_s contains all the sinks that are closest to s .

Theorem 2. *Let $s \in S$, $i \in T$ and $k \in K$ such that $\rho(s, i)$ and $\rho(i, k)$ are both finite. Then, if $k \in K_s$ and i lies on the shortest path from s to k ,*

$$\lim_{\mu \downarrow 0} \hat{\Phi}_{i,k}^s = \frac{[\mathbf{Q}_{ST} \mathbf{Q}_{TT}^{\rho(s,i)-1}]_{si} [\mathbf{Q}_{TT}^{\rho(i,k)-1} \mathbf{Q}_{TK}]_{ik}}{\sum_{k' \in K_s} [\mathbf{Q}_{ST} \mathbf{Q}_{TT}^{\rho(s,k)-2} \mathbf{Q}_{TK}]_{sk'}}. \tag{34}$$

Otherwise, $\lim_{\mu \downarrow 0} \hat{\Phi}_{i,k}^s = 0$.

Proof. Let $s \in S$, $i \in T$ and $k \in K$. Since, $\rho(s, i)$ and $\rho(i, k)$ are finite, it follows that $\rho(s, k)$ is also finite, that is, k is reachable from s through i and the normalized channel tensor $\hat{\Phi}$ is well defined for all $\mu \in (0, 1)$. Recall that

$$\hat{\Phi}_{i,k}^s = \frac{\Phi_{i,k}^s}{\Psi_s} = \frac{[\mathbf{P}_{ST} \mathbf{G}]_{si} [\mathbf{G} \mathbf{P}_{TK}]_{ik}}{\sum_{k' \in K} F_{sk'}} \tag{35}$$

where $F_{sk'} = \mathbf{P}_{SK} + \mathbf{P}_{ST}\mathbf{G}\mathbf{P}_{TK}]_{sk'}$.

Let $u, v \in T$ and let $d = \rho(u, v)$. It can be easily shown (see Lemma A.3 from (Stojmirović and Yu, 2007) for a partial proof) that $[\mathbf{P}_{TT}^n]_{uv} = 0$ for all $n < d$ and $[\mathbf{P}_{TT}^d]_{ij} > 0$. Therefore,

$$G_{uv} = \sum_{n=d}^{\infty} [\mathbf{P}_{TT}^n]_{uv} = \sum_{n=d}^{\infty} \mu^n [\mathbf{Q}_{TT}^n]_{uv} = \mu^d [\mathbf{Q}_{TT}^d]_{uv} + O(\mu^{d+1})$$

as $\mu \downarrow 0$. Hence,

$$\begin{aligned} [\mathbf{P}_{ST}\mathbf{G}]_{si} &= \sum_{j \in T} \mu^{\rho(j,i)+1} Q_{sj} [\mathbf{Q}_{TT}^{\rho(j,i)}]_{ji} + O(\mu^{\rho(j,i)+2}) \\ &= \mu^{\rho(s,i)} [\mathbf{Q}_{ST}\mathbf{Q}_{TT}^{\rho(s,i)-1}]_{si} + O(\mu^{\rho(s,i)+1}), \end{aligned} \quad (36)$$

$$\begin{aligned} [\mathbf{G}\mathbf{P}_{TK}]_{ik} &= \sum_{j \in T} \mu^{\rho(i,j)+1} [\mathbf{Q}_{TT}^{\rho(i,j)}]_{ij} Q_{jk} + O(\mu^{\rho(i,j)+2}) \\ &= \mu^{\rho(i,k)} [\mathbf{Q}_{TT}^{\rho(i,k)-1}\mathbf{Q}_{TK}]_{ik} + O(\mu^{\rho(i,k)+1}). \end{aligned} \quad (37)$$

Let $\xi = \rho(s, k'')$, where $k'' \in K_s$. We will consider the denominator of Equation (35) under two separate cases, $\xi = 1$ and $\xi > 1$.

If $\xi > 1$, for all $k' \in K$, the vertices s and k' are not adjacent and thus $P_{sk'} = 0$. Hence, since s and k' are connected, there exist $j, j' \in T$ such that $\rho(s, k') = \rho(s, j) + \rho(j, j') + \rho(j', k') = \rho(j, j') + 2$, implying

$$\begin{aligned} &[\mathbf{P}_{ST}\mathbf{G}\mathbf{P}_{TK}]_{sk'} \\ &= \sum_{j, j' \in T} \mu^{\rho(j,j')+2} Q_{sj} [\mathbf{Q}_{TT}^{\rho(j,j')}]_{jj'} Q_{j'k'} + O(\mu^{\rho(j,j')+3}) \\ &= \mu^{\rho(s,k')} [\mathbf{Q}_{ST}\mathbf{Q}_{TT}^{\rho(s,k')-2}\mathbf{Q}_{TK}]_{sk'} + O(\mu^{\rho(s,k')+1}). \end{aligned} \quad (38)$$

Therefore,

$$\Psi_s = \sum_{k' \in K} \mathbf{P}_{SK} + \mathbf{P}_{ST}\mathbf{G}\mathbf{P}_{TK}]_{sk'} \quad (39)$$

$$= \sum_{k' \in K_s} \mu^\xi [\mathbf{Q}_{ST}\mathbf{Q}_{TT}^{\xi-2}\mathbf{Q}_{TK}]_{sk'} + O(\mu^{\xi+1}), \quad (40)$$

and, as $\mu \downarrow 0$,

$$\hat{\Phi}_{i,k}^s \rightarrow \frac{\mu^{\rho(s,i)+\rho(i,k)} [\mathbf{Q}_{ST}\mathbf{Q}_{TT}^{\rho(s,i)-1}]_{si} [\mathbf{Q}_{TT}^{\rho(i,k)-1}\mathbf{Q}_{TK}]_{ik}}{\mu^\xi \sum_{k' \in K_s} [\mathbf{Q}_{ST}\mathbf{Q}_{TT}^{\xi-2}\mathbf{Q}_{TK}]_{sk'}} \quad (41)$$

By the triangle inequality and our assumptions on s, i and k ,

$$\rho(s, i) + \rho(i, k) \geq \rho(s, k) \geq \xi. \quad (42)$$

The first inequality becomes an equality if and only if i lies on the shortest path between s and k while the second is an equality if and only if $k \in K_s$. Therefore, if the assumption of the theorem is satisfied, the value of $\hat{\Phi}_{i,k}^s$ converges to the value of the right hand side of Equation (34), while otherwise $\lim_{\mu \downarrow 0} \hat{\Phi}_{i,k}^s = 0$.

On the other hand, if $\xi = 1$, $\Psi_s \rightarrow \sum_{k' \in K_s} \mu Q_{sk'} + O(\mu^2)$ and therefore, since $\rho(s, i) + \rho(i, k) \geq 2$, $\hat{\Phi}_{i,k}^s \rightarrow 0$ as $\mu \downarrow 0$. \square

We have therefore shown that, as $\mu \downarrow 0$, only the nodes associated with the shortest path from each source to the sink(s) closest to it will have positive values of the normalized channel tensor – all other entries will be exactly 0.

Theorem 3. *Let $s \in S$ and suppose the normalized channel tensor $\hat{\Phi}$ is well defined for all $\mu \in (0, 1)$. Then,*

$$\lim_{\mu \downarrow 0} \mathbb{E}(L_s) = \rho(s, k), \quad (43)$$

where $k \in K_s$.

Proof. Let $s \in S$, let $k \in K_s$ and let $d = \rho(s, k)$. For $m = 1, 2 \dots d - 1$, let $\Pi_s(m) = \{i \in T : \rho(s, i) = m \text{ and } \rho(s, i) + \rho(i, k) = d\}$. The set $\Pi_s(m)$ consists of all transient nodes that are at the distance m from s on a shortest path from s to any of the sinks closest to s . By Theorem 2,

$$\begin{aligned} & \lim_{\mu \downarrow 0} \sum_{k'' \in K} \sum_{i \in T} \hat{\Phi}_{i,k}^s \\ &= \sum_{k'' \in K_s} \sum_{m=1}^{d-1} \sum_{i \in \Pi_s(m)} \frac{[\mathbf{Q}_{ST} \mathbf{Q}_{TT}^{m-1}]_{si} [\mathbf{Q}_{TT}^{d-m-1} \mathbf{Q}_{TK}]_{ik''}}{\sum_{k' \in K_s} [\mathbf{Q}_{ST} \mathbf{Q}_{TT}^{\rho(s,k)-2} \mathbf{Q}_{TK}]_{sk'}} \\ &= \sum_{k'' \in K_s} \sum_{m=1}^{d-1} \sum_{i \in T} \frac{[\mathbf{Q}_{ST} \mathbf{Q}_{TT}^{m-1}]_{si} [\mathbf{Q}_{TT}^{d-m-1} \mathbf{Q}_{TK}]_{ik''}}{\sum_{k' \in K_s} [\mathbf{Q}_{ST} \mathbf{Q}_{TT}^{d-2} \mathbf{Q}_{TK}]_{sk'}} \\ &= \sum_{m=1}^{d-1} \frac{\sum_{k'' \in K_s} [\mathbf{Q}_{ST} \mathbf{Q}_{TT}^{d-2} \mathbf{Q}_{TK}]_{sk''}}{\sum_{k' \in K_s} [\mathbf{Q}_{ST} \mathbf{Q}_{TT}^{d-2} \mathbf{Q}_{TK}]_{sk'}} \\ &= d - 1. \end{aligned}$$

Therefore, by Equation (27),

$$\lim_{\mu \downarrow 0} \mathbb{E}(L_s) = 1 + \lim_{\mu \downarrow 0} \sum_{k'' \in K} \sum_{i \in T} \hat{\Phi}_{i,k}^s = \rho(s, k),$$

as required. \square \square

A.3 Applications

A possible application of the results of this section is to determine the damping factors for a context through specifying the average path length of random walks. For example, if a single source s is present, we can write $\mathbb{E}(L_s) = f(\mu)$ (where f is given by Equation (27)) and solve for any valid value of path length. Since f is continuous and increasing on $(0, 1)$, the required (possibly non-unique) value of μ can be easily found numerically.

If there are multiple sources within the context, one can specify the sum or a weighted average of path lengths of walks emitted from all of the sources and then solve for μ . Even finer application specific control may be possible by constraining damping at specific nodes as well as the general damping factor μ .

B Rapid Evaluation of Submatrix Inverses

Consider an invertible block matrix $\mathbf{M} = \begin{bmatrix} \mathbf{A} & \mathbf{B} \\ \mathbf{C} & \mathbf{D} \end{bmatrix}$, where \mathbf{A} is a square matrix. It is a well known result of linear algebra (see for example Poole (2005), chapter 3) that the inverse of \mathbf{M} can be written as

$$\mathbf{M}^{-1} = \begin{bmatrix} \mathbf{A}^{-1} + \mathbf{A}^{-1} \mathbf{B} \mathbf{Q}^{-1} \mathbf{C} \mathbf{A}^{-1} & -\mathbf{A}^{-1} \mathbf{B} \mathbf{Q}^{-1} \\ -\mathbf{Q}^{-1} \mathbf{C} \mathbf{A}^{-1} & \mathbf{Q}^{-1} \end{bmatrix}, \quad (44)$$

where $\mathbf{Q} = \mathbf{D} - \mathbf{C}\mathbf{A}^{-1}\mathbf{B}$. Suppose we are interested in computing matrices of the form $\mathbf{A}^{-1}\mathbf{U}$, where \mathbf{A} is very large and \mathbf{U} is an arbitrary matrix with appropriate number of rows. If it is necessary to perform a large number of such computations with different square submatrices \mathbf{A} (the matrix \mathbf{M} may be permuted in each case to reorder the indices), it could be effective to precompute the matrix \mathbf{M}^{-1} (or, computationally more appropriately, its LU-decomposition) once and in each case extract the required inverse \mathbf{A}^{-1} through simple and relatively inexpensive algebraic manipulations and permutations.

Indeed, write $\mathbf{M}^{-1} = \begin{bmatrix} \mathbf{X} & \mathbf{Y} \\ \mathbf{Z} & \mathbf{W} \end{bmatrix}$, with the blocks of the same size as in Equation (44), and observe that $\mathbf{W} = \mathbf{Q}^{-1}$ and hence $\mathbf{Y}\mathbf{W}^{-1}\mathbf{Z} = \mathbf{A}^{-1}\mathbf{B}\mathbf{Q}^{-1}\mathbf{C}\mathbf{A}^{-1}$. Therefore,

$$\mathbf{A}^{-1} = \mathbf{X} - \mathbf{Y}\mathbf{W}^{-1}\mathbf{Z}, \quad (45)$$

and thus

$$\mathbf{A}^{-1}\mathbf{U} = \mathbf{X}\mathbf{U} - \mathbf{Y}\mathbf{W}^{-1}\mathbf{Z}\mathbf{U}. \quad (46)$$

Since, by our assumption, the matrix \mathbf{W} is very small compared to \mathbf{A} , computing the inverse of \mathbf{W} and applying Equation (45) over many evaluations of \mathbf{A}^{-1} can be significantly faster than extracting the submatrix \mathbf{A} and computing its inverse directly each time. The cost of initial computation of \mathbf{M}^{-1} can be amortized over many evaluations of the inverse of the submatrices.

To evaluate of the matrix $\mathbf{A}^{-1}\mathbf{U}$, we compute the matrices $\mathbf{Y}\mathbf{W}^{-1}$ and

$$\mathbf{M}^{-1} \begin{bmatrix} \mathbf{U} \\ \mathbf{0} \end{bmatrix} = \begin{bmatrix} \mathbf{X} & \mathbf{Y} \\ \mathbf{Z} & \mathbf{W} \end{bmatrix} \begin{bmatrix} \mathbf{U} \\ \mathbf{0} \end{bmatrix} = \begin{bmatrix} \mathbf{X}\mathbf{U} \\ \mathbf{Z}\mathbf{U} \end{bmatrix}$$

and then produce $\mathbf{A}^{-1}\mathbf{U}$ using Equation (46).